Letters on Materials 15 (4), 2025 pp. 394-400 www.lettersonmaterials.com

Received 26 August 2025; Accepted 25 November 2025
https://doi.org/10.48612/letters/2025-4-394-400 https://elibrary.ru/hlfjte

# Patterns of changes in acoustic emission parameters during laser impact on superhard materials

M. P. Kozochkin, M. Sh. Migranov[†], S. V. Fedorov,

A. S. Gusev, E. A. Ostrikov, E. S. Mustafaev

[†]migmars@mail.ru

Moscow State University of Technology "STANKIN", Moscow 127055, Russia

**Abstract:** The study involved experimental investigations into the correlations between acoustic emission (AE) signal parameters and the processing regimes of laser, electro-discharge, and mechanical machining. Specifically, it presents the results of analyzing how AE signal parameters correlate with variations in laser pulse power and duration, as well as with processing productivity and the quality of the resulting surface. It is demonstrated that a change in the power density of the impact similarly affects the AE signal spectrum across different technologies, allowing this parameter to be used for assessing process state. Particular attention is paid to laser material probing, where AE signals reflect such phenomena as vapor-plasma plume formation, the energy of internal bonds in the material structure, and the self-focusing of laser radiation. The paper presents graphs illustrating the correlations between AE parameters and laser processing regimes for various materials. The study provides insights into the relationship between AE parameters and the process shifting towards either an increased proportion of melt in the removed material or towards its vaporization. This offers prospects for implementing real-time processing quality monitoring. The results demonstrate that AE parameters can serve as indicators of processing productivity, surface quality, and material properties. This opens up prospects for the industrial application of the method, for instance, in the real-time monitoring of processes involving concentrated energy flows, assessing the properties of new alloys, and optimizing technological regimes. The presented data indicate that AE parameters can be a tool for gaining deeper insights into the complex phenomena accompanying the impact of concentrated energy flows on materials.

**Keywords:** acoustic emission, signal spectrum, laser processing, ultra-hard materials, process monitoring, concentrated energy flows, power density, vapor-plasma plume, decay rate

***Acknowledgements:*** *The study was funded by the Russian Science Foundation grant No. 22-19-00670-P, https://rscf.ru/en/project/22-19-00670/.*

## 1. Introduction

The use of technologies based on processing with concentrated energy flows (hereinafter referred to as "energy flows") significantly broadens the possibilities for industrial application of components made from ultra-hard, heat-resistant, and difficult-to-machine materials. These technologies primarily include laser, electro-discharge, and electron-beam processing. It should be noted that understanding the kinetics of technological processes utilizing energy flows is considerably challenging due to their high speed, the small scale of the process core, and the difficulties in direct observation. The monitoring of acoustic signals accompanying technological processes offers a promising avenue in this direction.

Research into Acoustic Emission (AE) signals for non-destructive testing and process monitoring was actively conducted as early as the last century in academic institutes in Russia and Belarus, where methods for diagnosing rotary mechanisms were developed and contact processes during various types of friction were studied. AE application methods became a key factor in assessing the strength properties of materials [1]. Two failure scenarios were established: one involving the accumulation of plastic deformations throughout the volume, and another involving premature failure with the formation and growth of crack-like defects even before the material reaches its ultimate state [2–4]. Reference [1] states that AE analysis is founded on two main approaches: the first is related to continuum mechanics and uses averaged physical-mechanical parameters, while the second is linked to the physics of strength and plasticity in accordance with dislocation theory [5]. Currently, it can be stated that AE methods allow for a qualitative assessment of damage accumulation processes in a material and can provide a prognosis for the development of failure and its location [1,6].

Literature increasingly features AE research related to studying the processes of energy flow impact on various materials during laser, electro-discharge, and electron-beam processing. The goal of this research is to develop a set of AE characteristics that enable the assessment of real-time process quality to minimize end-product defects and for the timely adjustment of processing parameters [7–9]. AE signals are observed during phase transformations accompanied by changes in the material's crystal lattice, as well as during substance crystallization and melting. This fact has spurred research into the potential of acoustic monitoring for additive technologies, laser melting, and welding [10–12].

Experience shows that AE signal parameters can be applied not only for monitoring and control but also used as a tool for understanding the processes occurring within a material under the influence of energy flows [9]. Studies have emerged where the parameters of AE signals accompanying laser pulse impacts on a material's surface are used to evaluate the properties of the materials themselves [13,14]. In [13], the authors concluded that the magnitude of a material's critical energy density affects the AE pattern during laser action. The authors of [14] proceed from this assumption, investigating AE signals during the impact of laser pulses on various tooling materials.

The rapid development of research related to the creation of new composite materials and alloys has led to a search for effective methods to evaluate their properties for selecting formation regimes and optimizing component composition [15–17].

For many years, Moscow State Technological University "STANKIN" has focused on monitoring the condition of tools in blade machining. Incorporating research into the relationship between AE parameters and the characteristics of thermal flow impact on materials has enabled the comparison of AE parameter changes across these technologies and blade machining, identifying similarities and differences in their behavior [18,19].

The aim of this work is to study the prospects of using AE for testing the properties of new alloys with energy flows and for monitoring technologies that utilize thermal flows. A review of the literature and the authors' own research demonstrate that AE monitoring can serve as a tool for understanding the kinetics of a wide range of technological processes and can be used for their improvement [12,18].

## 2. Theoretical and experimental background

The commonality of AE parameter relationships in traditional cutting and CEF processing. When examining the response of AE parameters to changes in power density (PD) of energy input across different technologies, it can be observed that both blade processing and CEF processing exhibit similar trends in AE parameters. In blade processing, PD decreases with tool wear due to the increased area through which energy is transferred to the workpiece. Across different technologies, an increase in PD causes a predominant growth of high-frequency components in the AE signal relative to low-frequency components [12,13].

Figure 1 shows graphs depicting changes in the *Kf* parameter (ratio of amplitudes in low and high-frequency bands) of the AE signal during blade and laser processing of steel surfaces. In Fig. 1a, the *Kf* parameter represents the ratio of RMS amplitudes in the 0.5–3 kHz and 6–16 kHz bands. PD increases with cutting speed (*Kf* decreases) and decreases with tool wear, which depends on the number of processed parts (*Kf* increases). In Fig. 1b, PD ($q_s$) increases through higher laser pulse power while maintaining a constant focal spot. Here, the RMS amplitudes of AE signals in the 8 kHz and 16 kHz octaves increase monotonically, but the growth is faster in the 16 kHz octave, resulting in a decrease of *Kf* with increasing $q_s$. Monitoring *Kf* enables the assessment of real-time PD changes during various technological processes and allows for necessary adjustments to operating parameters.

Figure 2 shows examples of changes in AE parameters during turning and electro-discharge machining. The changes in the octave and 1/3-octave AE spectra are illustrated for the following conditions: at the start of machining with a sharp tool (Fig. 2a), in clean working fluid (Fig. 2b), and at the end of the process when the cutting edge is worn and the concentration of erosion products is elevated.

A comparison of the spectra in Fig. 2 reveals their similarity regarding the change in amplitudes at high and low frequencies with a decrease in $q_s$. The commonality between mechanical and electro-discharge machining processes is linked to the analogous direction of changes in $q_s$ as the conditions for removal of the processed material deteriorate. In blade machining, tool wear reduces $q_s$ and complicates the formation of cracks that separate the chips. As a result, the duration of the load-unload impulse within the elastic system increases. This increase in impulse duration distorts the AE spectrum, leading

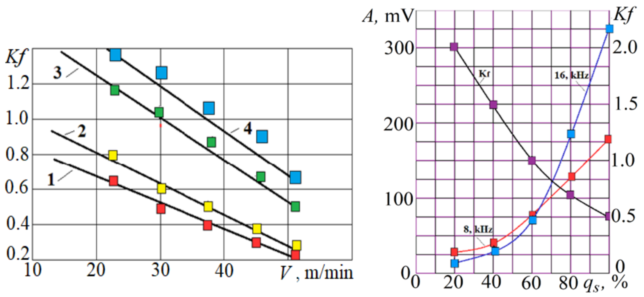


a b

**Fig. 1.** (Color online) Changes in AE parameters with decreasing power density during turning and electro-discharge machining: processing of a series of workpieces made of steel KhN77TYuR (NiCr20TiAl) at different speeds (1 — first workpiece; 2 — 4th workpiece; 3 — 27th workpiece; 4 — 35th workpiece) (a); impact of laser pulses with different power densities $q_s$ on a steel workpiece (change in RMS amplitude in the 8 and 16 kHz octave bands and their ratio *Kf*) (b).

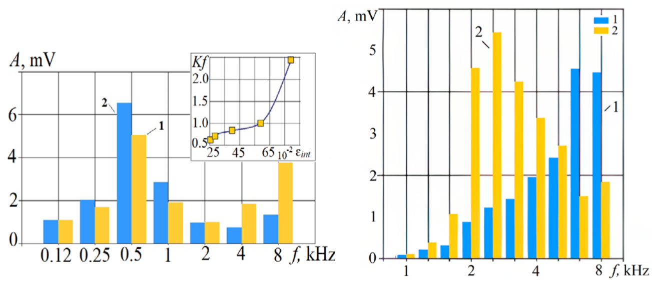


a b

**Fig. 2.** (Color online) Changes in AE parameters with a decrease in $q_s$ during turning and electro-discharge machining: octave AE spectra during turning with a sharp (1) and a worn (2) cutting tool (a); 1/3-octave spectra during electro-discharge machining in clean working fluid (1) and with the accumulation of erosion products (2) (b). The inset shows an increase in *Kf* with the growth of wear and deformation ($\varepsilon_{int}$) of the surface layer.

to a rise in the *Kf* ratio of amplitudes in the low-frequency to high-frequency range. In electro-discharge machining, an increase in the concentration of erosion products within the gap occurs. A portion of the discharge energy is then diverted from processing the surface to the breakdown of these erosion products. This reduces the fraction of discharge power reaching the workpiece, i.e., $q_s$ decreases [18]. Consequently, the proportion of vaporized material is reduced while the proportion of melt increases, resulting in the formation of impulses that are more extended in time.

## 3. Equipment and methods of experimental research

Research into the relationship between AE parameters and the productivity of laser pulses has established that AE energy is monotonically related to the intensity of disturbing actions on the machine tool's elastic system during material removal [14,17]. Figure 3 shows a test bench for laser probing of various compositions of hard alloys and ceramics, along with a table of data obtained from experiments with the T15K6 alloy [17].

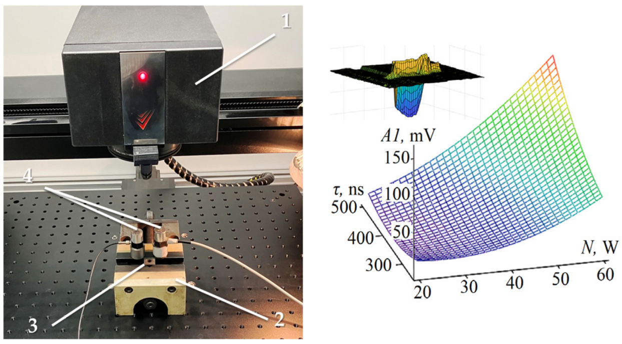


a b

**Fig. 3.** (Color online) "SharpMark Fiber GT 60" Laser System (a): 1 — laser module; 2 — sample holder; 3 — T15K6 alloy workpiece; 4 — AP2037–100 accelerometers. The graph (b) shows the dependence of the AE signal amplitude ($A_1$) in the 10–28 kHz range on the laser pulse power ($N$) and duration ($\tau$). Above the graph is a profilometer image of the resulting crater.

## 4. Results of experimental studies and their analysis

The experiments utilized a pulsed fiber laser with a wavelength of 1064 nm, a power of up to 60 W, and pulse durations ranging from 2 to 500 ns. An accelerometer with a transduction coefficient of 100 mV/G was employed. Data acquisition was performed using Matcard 14 software. Data on the geometry and volume of the craters were obtained using a Dektak XT stylus profiler.

A series of 12 experiments with different values of $N$ and $\tau$ was conducted. For each parameter set, a line of 10 craters was produced by delivering 5 pulses per crater. Figure 3 shows an example of a crater image obtained with the profiler. Using experimental design methodology, mathematical models and graphs illustrating the relationship between AE parameters and laser pulse duration and power were obtained.

The graph in Fig. 3 presents the dependence $A_1(N,\tau)$ in a general form. It is evident that an increase in both laser power and pulse duration leads to a monotonic rise in the AE amplitude in the 10–28 kHz frequency band. The influence of power is more pronounced. The nature of the presented dependencies is such that $A_1(N,\tau)$ can be approximated by a linear function with minimal error in the power range above 30 W. Similar dependencies were plotted for the AE signal in the 32–70 kHz range. While differing quantitatively, the trend of monotonic growth remains.

Based on the measurements of the crater shapes and volumes ($Q$), graphical representations of the dependence $Q(N,\tau)$ were constructed and are presented in Fig. 4.

The graphs in Fig. 4 are very similar to the graph in Fig. 3. By analogy with Fig. 3, the dependence of volume $Q$ on power is more pronounced here, just as it is for $A_1$. Pulse duration also influences the volume change, but significantly weaker than power.

To compare the dependencies in Figs. 3 and 4, the values of $A_1$ and $Q$ were expressed as percentages of their maximum values obtained in the experiments. This allows the normalized dependencies $A_{1_p}(N,\tau)$ and $Q_p(N,\tau)$ to be compared graphically or via their mathematical models. The linearization of the $A_{1_p}(N,\tau)$ and $Q_p(N,\tau)$ dependencies showed that this operation increases the discrepancy with the experimental data, but the error remains within 9% for both dependencies. The resulting planes cannot be considered parallel, but for practical purposes, this assumption is acceptable.

The ratio between the volume of extracted material and the volume of material ejected onto the surface around the crater is an important indicator. At low $q_s$, the proportion of material in the form of melt increases, forming surface irregularities. As a result, the roughness increases. As shown in Fig. 1b, monitoring $q_s$ can be performed by observing the current value of the *Kf* parameter.

Figure 5 shows a graphical representation of the relationship between the volume of material ejected ($V$) onto the surface as a percentage of the crater volume ($Q$), obtained under different laser processing regimes.

The graphs in Fig. 5 indicate that the proportion of ejected material decreases with increasing power and pulse width. Acoustics of Laser Probing. This section examines the influence of the processed material on the AE signals during laser exposure. This is important for developing new alloy compositions, as this method can provide prompt information about the properties of new samples.

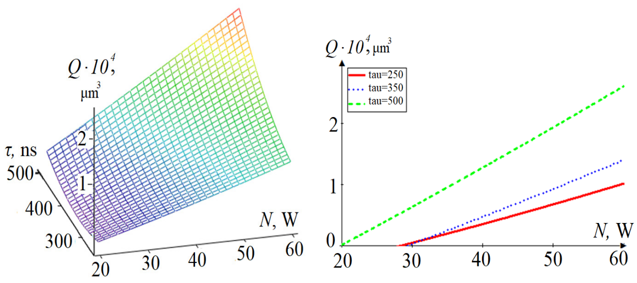


a b

**Fig. 4.** (Color online) Graphs of the dependence $Q(N,\tau)$: general view of the dependence (a); projections of the contour lines onto the coordinate planes at sections with constant $\tau$ values (b).

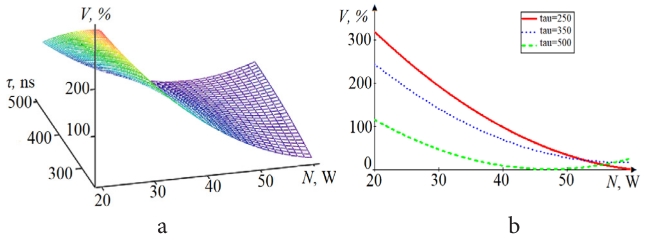


**Fig. 5.** (Color online) Graphs of the dependence $V(N,\tau)$ as a percentage of $Q$: general view of the dependence (a); projections of sections with identical pulse width values (b).

*Feature 1:* Formation of a Vapor-Plasma Plume above the Laser Interaction Zone. A laser pulse impacting the material causes heating, melting, and evaporation. Intensive evaporation generates a recoil wave within the material. At high radiation intensities, a plasma plume can form in the material's vapors. Depending on its temperature and density, the plasma influences the physics of the processing, as it can absorb or reflect the laser radiation, shielding the material and altering the kinetics of the thermal processes [19]. This property of the plasma plume affects the pulse productivity and the AE parameters. Different materials form a vapor-plasma cloud at different rates and with different properties. The rate of AE amplitude decay depends on the processed material and the distance between the craters. When craters are closely spaced, the plasma from adjacent craters affects the AE attenuation rate at the processing point.

Figure 6 shows the recorded AE signals during the formation of several craters, produced by delivering 200 laser pulses per crater (60 W, 500 ns, 10 kHz) on an aluminum alloy and $Al_2O_3$ ceramic. The figure displays the signal recordings only for the first two craters.

Figure 6 shows that for the aluminum alloy, the amplitude drops to the noise level within 4 ms, whereas for the ceramic, the decrease is barely noticeable. The decay rate ($\delta$) is conveniently expressed in %/ms, as illustrated in the sketch in Fig. 6a. When craters are closely spaced, the vapor-plasma cloud from adjacent craters affects the AE decay rate at the processing point. Figure 6c shows the dependencies of the AE decay rate in the 45–95 kHz range during the processing of the T15K6 hard alloy under the same conditions; 200 pulses were sequentially delivered into 24 craters, and this pass was repeated 5 times. It follows from Fig. 6c that the influence of the vapor-plasma cloud disappears only when the step $\Delta$ is increased to 80 μm. The vapor-plasma formation is stable over time: the period from one pass to the next was 0.5 seconds, yet its influence persists.

Table 1 shows the estimated AE decay rates for different input pulse powers for various tooling materials.

Table 1 shows that the AE attenuation rates for superhard materials are similar, but they are significantly lower than those of the T15K6 hard alloy. For aluminum alloys, it can reach 35–40%/ms under similar conditions. The evaluation of the attenuation rate for new alloy variants, classified as experimental high entropy alloys (HEA), yielded the following results for the 45–95 kHz range in %/ms:
No. 1 — Ti10-Zr40-Cr10-Ni10-W10-Mo10-Nb10 ($T$=1100°C) — 38;
No. 2 — Ti10-Zr40-Cr10-Ni10-W10-Mo10-Nb10 ($T$=1000°C) — 28;
No. 3 — Ti42-Zr12-Cr12-Ni12-Mo10-Nb12 — 32.
It is evident that HEA exhibit AE signal attenuation rates similar to those of alloys like T15K6.

*Feature 2:* Energy of Internal Bonds in the Material Structure. The latent bond energy between elementary particles in metals characterizes their mechanical properties [20]. Destructive factors act to break these bonds, while the internal energy of attraction between particles, which determines the material's strength characteristics, counteracts this. During laser exposure, material particles acquire sufficient energy to break the restraining bonds and leave the solid body as part of the vapor-plasma cloud. The solid body experiences a disturbing effect from the ejected vapor in the form of recoil impulses, as well as impulses arising within the solid body after the destruction of the restraining bonds in a certain volume. The unbroken bonds are forced to reconfigure to restore force equilibrium at the boundaries of the formed crater. The size of the resulting crater provides significant information about the strength characteristics of

**Table 1.** AE attenuation rate during pulse application to a single crater (%/ms).

| Material | | T15K6 (TiC+W) | | $Al_2O_3$ | | BOK60($Al_2O_3$+TiC) | | Sialon ($Si_3N_4$+ $Al_2O_3$) | |
|---|---|---|---|---|---|---|---|---|---|
| Power | | 60 W | 30 W | 60 W | 30 W | 60 W | 30 W | 60 W | 30 W |
| Frequency | 5–35 kHz | 24.1 | 29.4 | 2.06 | 4.92 | 4.0 | 4.7 | 1.9 | 1.4 |
| | 35–75 kHz | 26.0 | 19.4 | 2.44 | 5.0 | 4.1 | 4.5 | 3.1 | 2.9 |

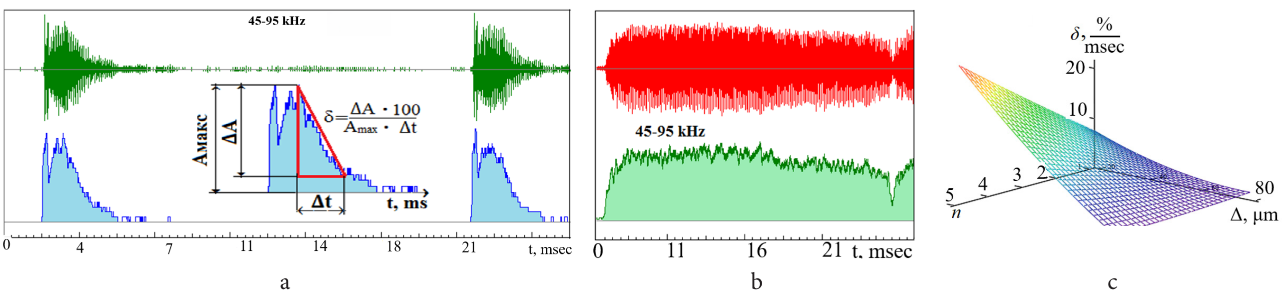


**Fig. 6.** (Color online) Examples of AE signal recordings (upper traces) in the 45–95 kHz range and their envelopes during the delivery of 200 laser pulses into a single crater: aluminum alloy (a); $Al_2O_3$ ceramic (b); dependence of the AE signal amplitude decay rate ($\delta$) on the distance between craters ($\Delta$) and the pass number ($n$) (c).

the sample. Figure 7 shows example profilometer images of craters for two materials: polycrystalline diamond with 90% diamond content (PCD90) and for Alloy No. 2 (see above).

Figure 7 provides examples of crater images for two materials with different properties. Rows of 10 craters were formed using laser pulses, with 5 pulses per crater. The pulse parameters were: power 60 W, duration 500 ns, frequency 10 kHz. The figure shows a close-up of one crater and a side view of the crater row. A difference in crater sizes and the amount of material ejected onto the surface is immediately visible. For PCD90, the height of the ejecta is less than 10% of the crater depth, while for HEA No. 2, it is already 30%. This indicates the high kinetic energy of PCD90 particles, which allows them to overcome restraining bonds and transition into vapor and plasma.

Table 2 presents data on the crater volumes obtained from laser pulse impact on different materials. It also provides the RMS amplitudes of AE in the 45 – 95 kHz range and the specific AE amplitudes, calculated as the ratio of amplitudes to crater volumes.

Table 2 presents an estimate of the internal energy in the form of the specific AE amplitude in the 45 – 95 kHz range. The energy of the acoustic signal is proportional to the square of the amplitude, but to avoid an extra computational step, Table 2 provides the values of specific amplitudes. Among the presented materials, the PCD94 sample possesses the highest internal energy. This is evident across all three indicators: the highest AE amplitude, the smallest volume of material removed during laser probing, and the highest specific amplitude.

**Table 2.** Crater volumes and AE amplitudes in experiments with different materials.

| Material sample | Average RMS AE amplitude in 45 – 95 kHz range ($A$, mV) | Average crater volume ($V$, μm$^3$) | Specific RMS amplitude ($A/V \times 10^{-3}$, mV/μm$^3$) |
|---|---|---|---|
| $Al_2O_3$ | 46.3 | 18060 | 2.56 |
| $PCD_{90}$ | 49.5 | 15762 | 3.14 |
| $PCD_{94}$ | 76.0 | 15690 | 4.84 |
| BN | 56.6 | 18842 | 3.00 |
| KNB | 56.6 | 18842 | 3.00 |
| T15K6 | 15.4 | 30612 | 0.50 |
| No. 1 | 4.84 | 52230 | 0.09 |
| No. 2 | 4.80 | 47708 | 0.103 |
| No. 3 | 4.00 | 47344 | 0.085 |

*Feature 3:* Reflection of laser radiation self-focusing in AE parameters. The presence of a vapor-plasma formation leads to another feature reflected in the AE signals. The initial sections of the article provided examples showing that the *Kf* parameter decreases with an increase in PD and rises with its reduction. The emergence of a vapor-plasma cloud during the impact of a large series of laser pulses into a single crater leads to the absorption of laser energy and a decrease in AE amplitudes across all frequency ranges. Figure 8 shows an example of AE signal recordings in two frequency ranges during the formation of a series of craters on a PCD94 plate (the first crater is shown) by delivering 200 pulses into each of them (60 W, 500 ns, 10 kHz).

The decrease in AE amplitude in Fig. 8 indicates a loss of energy in the laser pulses, a drop in productivity, and a reduction in $q_s$ (while the focal spot area remains constant). As shown in Fig. 1b, a decrease in the $q_s$ of laser radiation typically leads to an increase in *Kf*. However, Fig. 8b shows that *Kf* decreases by almost 50% during each processing period. To increase $q_s$ when the pulse power itself decreases, the focal spot area must be reduced. Thus, the AE parameters reveal the phenomenon of self-focusing. This phenomenon is well-known; in 1988, a group of physicists was awarded the Lenin Prize for its discovery. The nonlinear medium of the vapor-plasma plume acts as a converging lens [21 – 23]. If the energy reaching the workpiece surface decreases, but the focal spot area decreases at a faster rate, then $q_s$ can actually increase. It has been established that a laser beam passing through the vapor-plasma cloud medium alters the cloud's properties. As a result, the path of the beam itself becomes curved. If the refractive index within the beam's field increases or decreases, a corresponding concentration or scattering of energy is observed. When the rays are deflected towards the beam axis, the focal spot diameter decreases, giving rise to

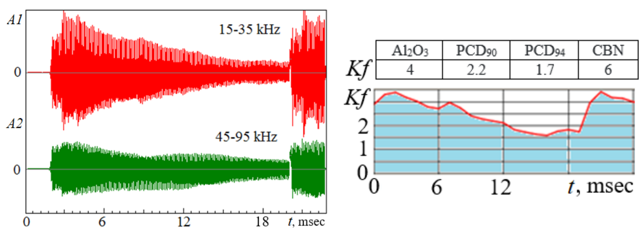


a b

**Fig. 8.** (Color online) Example of AE recordings in two frequency ranges during the formation of a series of craters on a $PCD_{94}$ plate using 200 laser pulses: recording in the 15 – 35 kHz and 45 – 95 kHz ranges (a); change in *Kf* during the processing of the first crater; the table shows the minimum *Kf* values for different materials (b).

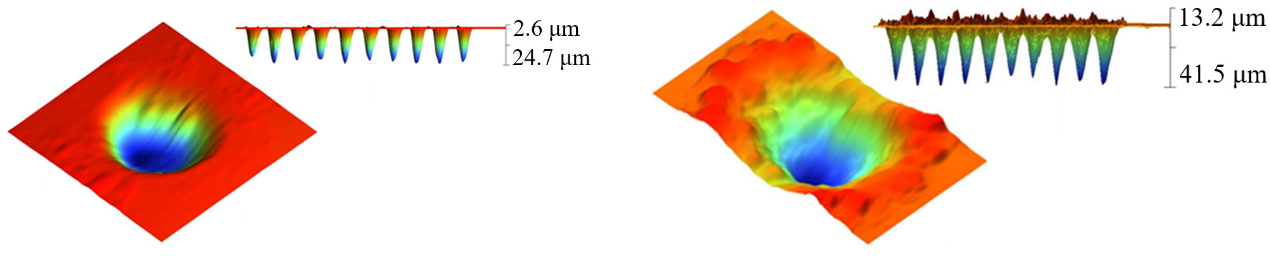


a b

**Fig. 7.** (Color online) Example images of craters obtained on a profiler for two material samples: made from $PCD_{90}$ (a); made from alloy No. 2 (b).

self-focusing; the nonlinear medium of the vapor-plasma cloud effectively becomes a converging lens.

The phenomenon of self-focusing is closely related to the effect of laser filamentation, which involves the localization of laser radiation energy within a thin filament characterized by high $q_s$ [23]. This occurs due to self-focusing within the nonlinear medium of the laser-induced plasma. While the specific material property reflected by the self-focusing phenomenon cannot yet be precisely identified, experimental results with ultra-hard materials indicate that this effect occurs more frequently in these materials under laser exposure. The table in Fig. 8b presents the *Kf* values obtained from experiments involving a series of laser pulses delivered into a single crater for different materials. It displays the minimum *Kf* values from the entire sequence during the laser exposure period. These data reveal that the minimum *Kf* values correspond to the PCD94 sample, which had also previously stood out in a series of other indicators in Table 2.

## 5. Conclusions

A review of the literature has shown that research into the potential uses of acoustic emission (AE) for process monitoring, product quality control, and equipment diagnostics is being conducted in all industrially developed countries. While work in the field of acoustic monitoring for traditional blade machining has been underway for a relatively long time, a marked increase in research activity concerning AE applications for processing with concentrated energy flows has been clearly observed over the last two decades. This surge is linked to the rapid development of additive technologies and methods for creating high-entropy alloys, which possess unique properties not found in traditional alloys. The sharp rise in demand for AE application in energy flow processing is explained by the fact that most conventional monitoring and control methods are simply unsuitable for use with these technologies. The most prominent areas of AE application include: additive manufacturing, laser cladding, laser welding, monitoring crack initiation and other defects, and assessing the properties of resulting alloys and components. A distinctive feature of this research direction is the attempt to implement artificial intelligence, neural networks, and the active use of machine learning. In the future, control systems should be capable of learning from incoming data without explicit programming. However, this requires large volumes of experimental data and efficient information sources. AE is considered one of the most sensitive and promising sources for this purpose. In light of the above, the present work falls within a highly relevant field related to the monitoring of energy flow processing. The originality of the research lies in the search for commonalities in AE parameter behavior across different types of technological operations. In particular, it was established that changes in power density similarly affect the deformation of the AE amplitude spectrum. This allows AE signals to be considered as a tool for monitoring and understanding not only traditional blade machining processes but also beam-based technologies. The study provides insights into the relationship between AE parameters and the current productivity of the laser processing, as well as the shift of the process towards an increased proportion of melt in the removed material or towards its vaporization. This opens prospects for implementing real-time processing quality monitoring. The article also demonstrates the possibility of using parameters of the vapor-plasma plume generated by laser exposure, specific AE amplitude, and the acoustic parameter *Kf* for the rapid assessment of new alloy compositions. Despite the abundance of AE research, the consideration of these specific parameters together is presented here for the first time.

## References


1. N.A. Semashko, V.I. Shport, B.N. Mar'in, Acoustic Emission in Experimental Materials Science, Moscow, Mashinostroenie, 2002, 239 p. (in Russian)
2. M.M. Kristal, A.Yu. Vinogradov, E.D. Merson, A.A. Eremichev, D.L. Merson, Effect of strain rate on acoustic emission during hydrogen assisted cracking in high carbon steel, Materials Science and Engineering: A. 550 (2012) 408 – 417.
3. V.M. Goritskii, Diagnostics of Metals, Moscow, Metallurgizdat, 2004, 402 p. (in Russian)
4. V.I. Ivanov, V.A. Barat, Acoustic-Emission Diagnostics. Moscow, Spektr, 2017, 362 p. (in Russian)
5. V.M. Pestrikov, E.M. Morozov, Fracture Mechanics of Solids, St. Petersburg, Professiya, 2002, 300 p. (in Russian)
6. V.G. Kharebov, A.V. Zhukov, A.V. Kuz'min, Practical evaluation of the acoustic emission method on process pipelines, In the World of Non-Destructive Testing 3 (41) (2014) 24 – 26. (in Russian)
7. M. Seleznev, T. Gustmann, J. Seyffer, U. Peuker, U. Kühn, J. Hufenbach, H. Biermann, A. Weidner, In situ detection of cracks during laser powder bed fusion using acoustic emission monitoring, Addit. Manuf. Lett. 10 (2022) 100099.
8. D. Kouprianoff, I. Yadroitsava, A. Plessis et al., Monitoring of Laser Powder Bed Fusion by Acoustic Emission: Investigation of Single Tracks and Layers, Front. Mech. Eng. 7 (2021) 1–17.
9. S.N. Grigoriev, M.P. Kozochkin, M.A. Volosova, A.A. Okunkova, S.V. Fedorov, Vibroacoustic Monitoring Features of Radiation-Beam Technologies by the Case Study of Laser, Electrical Discharge, and Electron-Beam Machining, Metals 11 (2021) 1117.
10. K.A. Stepanova, D.O. Kuzivanov, A.V. Fedorov, I.Yu. Kinzhagulov, Acoustic emission images of direct laser deposition, Optoelectron. Instrum. Data Process. 60 (2024) 109 – 115. (in Russian)
11. C. Chua, Y. Liu, R.J. Williams, C.K. Chua, S.L. Sing, In-process and post-process strategies for part quality assessment in metal powder bed fusion: a review, J. Manuf. Syst. 73 (2024) 75 – 105.
12. P.R. Prem, A.P. Sanker, S. Sebastian, et al., A review on application of acoustic emission testing during additive manufacturing, J. Nondestr. Eval. 42 (2023) 96.
13. S.D. Zotov, A.A. Kuznetsov, A.A. Lebedev, E.N. Lotkova, Non-reproducibility of acoustic emission during cyclic irradiation of solids by an infrared laser pulse, Short Commun. Phys. Lebedev Phys. Inst. (2017) 3 – 9. (in Russian)

14. M.P. Kozochkin, S.V. Fedorov, M.Sh. Migranov, E.A. Ostrikov, A.S. Gusev, Relationships between parameters of acoustic emission signals and features of material processing, Control. Diagn. 28, 10 (2025) 25 – 40. (in Russian)
15. G. A. Baglyuk, Yu. G. Bezymyanny, O. V. Tal'ko, Display of properties and structural features of powder hot-stamped composites based on the analysis of acoustic fields, in: Technical Acoustics: Developments, Problems, Prospects. Proc. Int. Sci.-Pract. Conf. (Vitebsk, May 2021), Vitebsk State Technological University, Vitebsk, 2021, pp. 69 – 71. (in Russian)
16. Yu.G. Sokolovskaya, N.B. Podymova, A.A. Karabutov, Laser opto-acoustic method for the quantitative evaluation of the porosity of carbon-fiber-reinforced plastics by measuring their acoustic impedance, Acoust. Phys. 66 (2020) 86 – 94. (in Russian)
17. V.K. Merinov, V.V. Kozhushko, V.P. Sergienko, A.Ya. Grigoriev, Laser opto-acoustic diagnostics of metal-polymer composite joints, in: Technical Acoustics: Developments, Problems, Prospects. Proc. Int. Sci.-Pract. Conf. (Vitebsk, May 2021), Vitebsk State Technological University, Vitebsk, 2021, pp. 56 – 58. (in Russian)
18. S.N. Grigoriev, M.P. Kozochkin, A.N. Porvatov, S.V. Fedorov, A.P. Malakhinsky, Investigation of the Information Possibilities of the Parameters of Vibroacoustic Signals Accompanying the Processing of Materials by Concentrated Energy Flows, Sensors 23 (2023) 750.
19. S.N. Grigoriev, M.P. Kozochkin, A.N. Porvatov, E.A. Ostrikov, E.S. Mustafaev, V.D. Gurin, A.A. Okunkova, Acoustic Features of the Impact of Laser Pulses on Metal-Ceramic Carbide Alloy Surface, Sensors 24 (2024) 5160.
20. N.V. Vinogradova, M.A. Prokofiev, Relationship Between Latent Deformation Energy and Technological Conditions of Mechanical Processing, Strengthening Technol. Coat. 1 (2011) 3 – 7. (in Russian)
21. O.G. Kosareva, N.A. Panov, Physics of Laser Filaments, Moscow University Press, Moscow, 2021, 153 p. (in Russian)
22. I. Yu. Letyagin, K. V. Felikan, V. Ya. Belenkiy, A. P. Erikov, Investigation of parameters of plasma formed in the zone of laser welding in vacuum, Bulletin PNRPU Mech. Eng. Mater. Sci. 23 (2021) 60 – 65. (in Russian)
23. I. Yu. Letyagin, V. Ya. Belenkiy, D. N. Trushnikov, S. Pang, Analysis of the amplitude-time parameters of current pulses in a plasma during laser beam welding, IOP Conf. Ser.: Mater. Sci. Eng. 759 (2020) 012015.